Supporting Information for:

Multiform La_2O_3: Yb^{3+}/Er^{3+}/Tm^{3+} Submicro-/Microcrystals Derived from Hydrothermal Process: Morphology Control and Tunable Upconversion Luminescence Properties

Guogang Li, Mengmeng Shang, Dongling Geng, Dongmei Yang, Chong Peng, Ziyong Cheng, and Jun Lin*

State Key Laboratory of Rare Earth Resource Utilization Changchun Institute of Applied Chemistry, Chinese Academy of Sciences, Changchun 130022 (P. R. China), and Graduate School of the Chinese Academy of Sciences, Beijing 100049 (P. R. China).

* Address correspondence to jlin@ciac.jl.cn

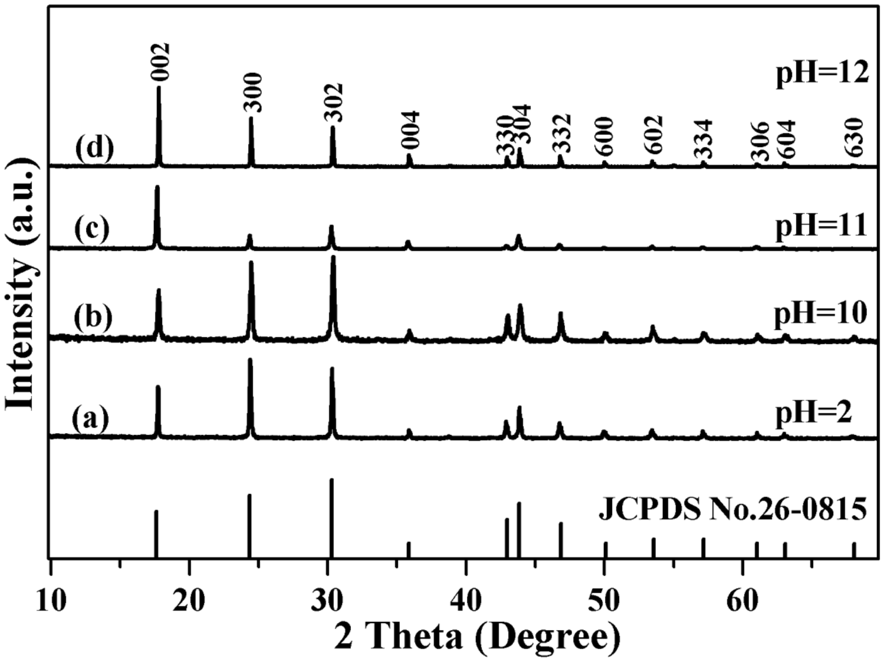

Figure S1. XRD patterns of the as-prepared $LaCO_3OH$ products (V_{EG/H_2O} = 1:3, $C_{CO(NH_2)_2}$ = 6.25 mol·L^{-1}) at 180 ^{o}C for 24 h with different pH values of (a) 2, P4; (b) 10, P5; (c) 11, P6; (d) 12, P7 and the standard data of $LaCO_3OH$ (JCPDS card no. 26-0815).

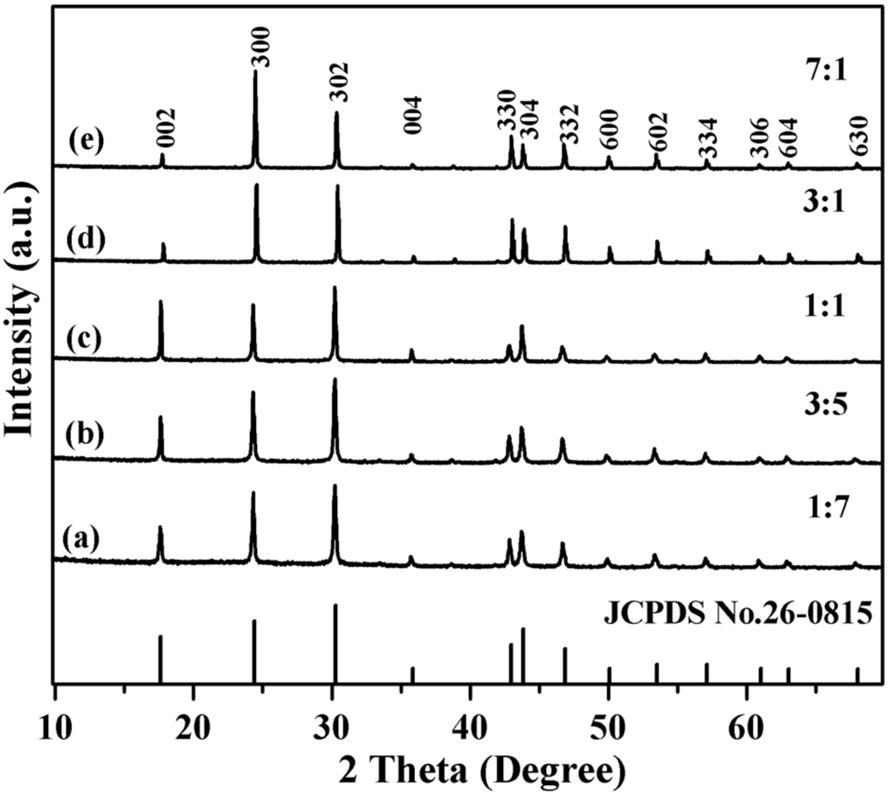

Figure S2. XRD patterns of the as-prepared $LaCO_3OH$ products (pH = 10, $C_{CO(NH_2)_2}$ = 6.25 mol·L^{-1}) at 180 °C for 24 h with different V_{EG/H_2O}: (a) 1:7, P11; (b) 3:5, P12; (c) 1:1, P13; (d) 3:1, P14; (e) 7:1, P15 and the standard data of $LaCO_3OH$ (JCPDS card no. 26-0815).

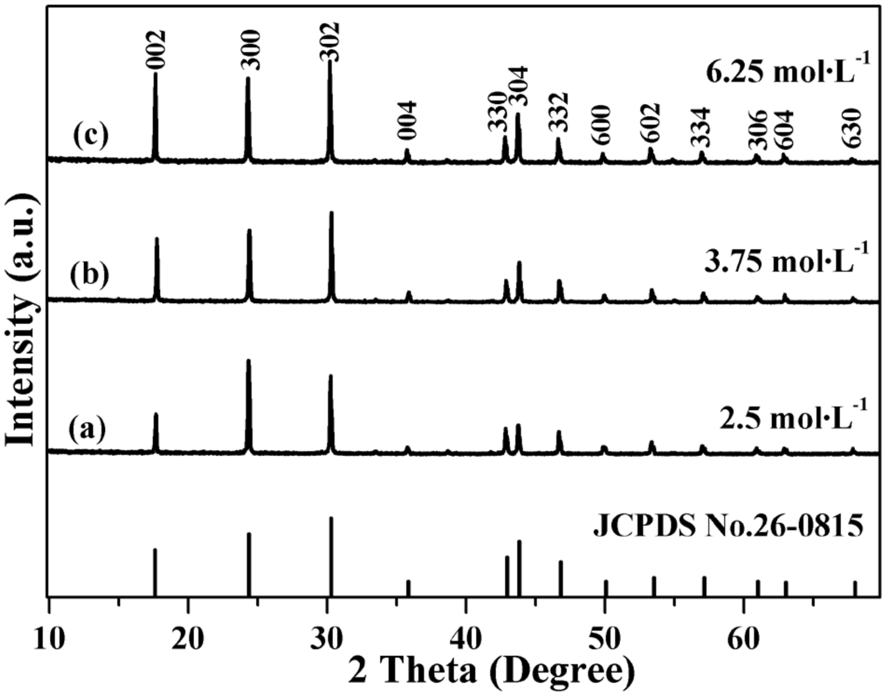

Figure S3. XRD patterns of the as-prepared $LaCO_3OH$ products (pH = 10, V_{EG/H_2O} = 1:3) at 180 ^{o}C for 24 h with different $C_{CO(NH_2)_2}$: (a) 2.5, P16; (b) 3.75, P17; (c) 6.25, P18 mol·L^{-1} and the standard data of $LaCO_3OH$ (JCPDS card no. 26-0815).

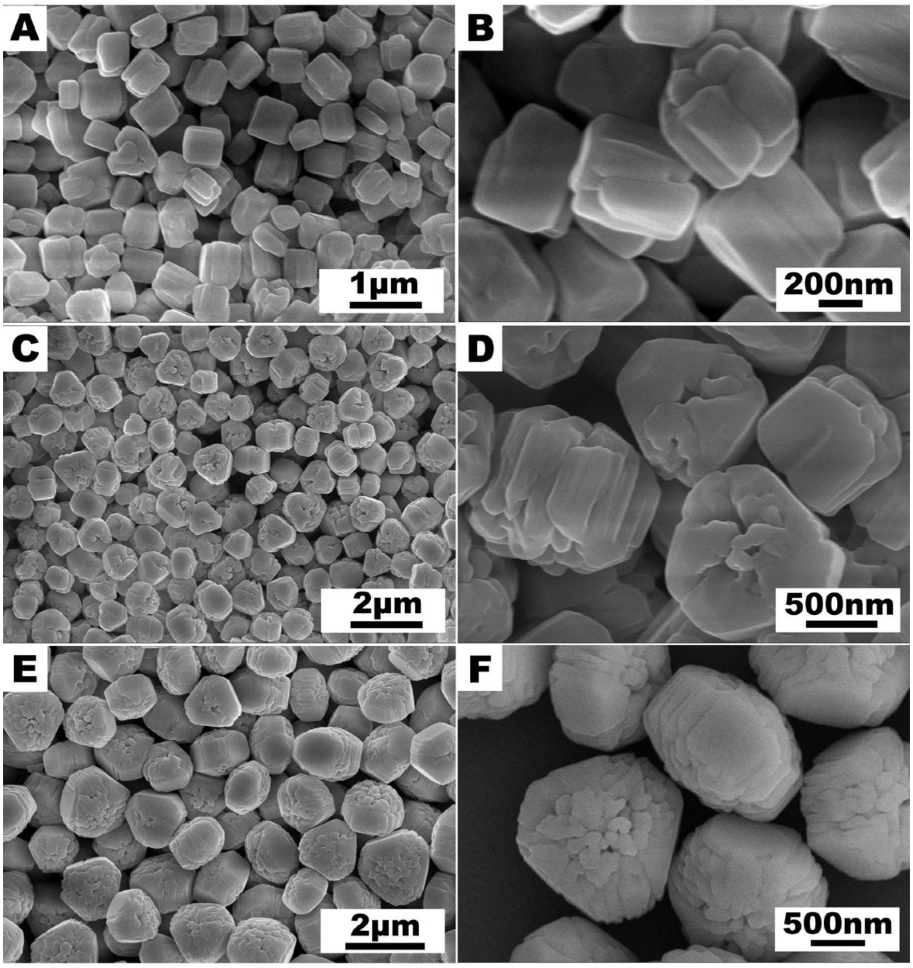

Figure S4. The influence of the dosages of $CO(NH_2)_2$ ($C_{CO(NH_2)_2}$) on the shapes of $LaCO_3OH$ products when fixing pH = 10, V_{EG/H_2O} = 1:3. (A, B) 2.5 mol·L^{-1}; (C, D) 3.75 mol·L^{-1} and (E, F) 6.25 mol·L^{-1}.

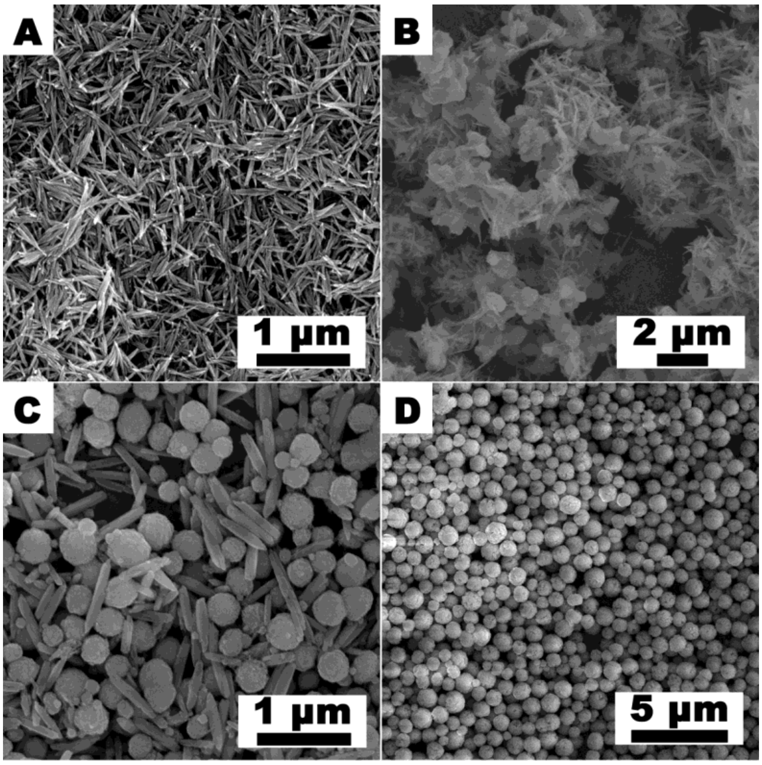

Figure S5. Typical SEM images of the representative P1 obtained at 180 ^{o}C at early stages with the reaction durations: (A) 10 min, (B) 30 min, (C) 1 h and (E) 4 h.

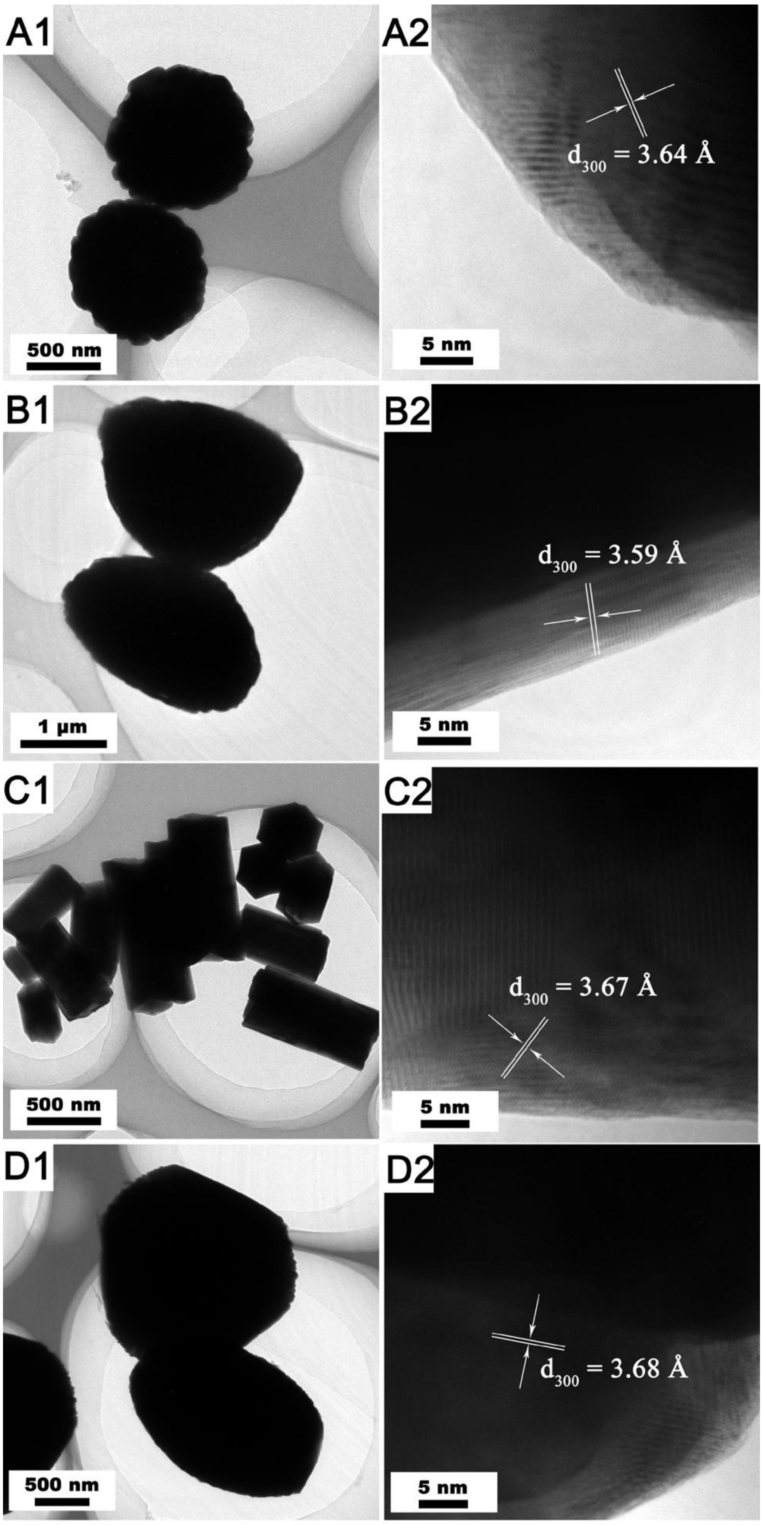

Figure S6. Typical TEM images of (A1) P2, (B1) P6, (C1) P8 and (D1) P13, respectively. (A2-D2) are their corresponding HRTEM images.

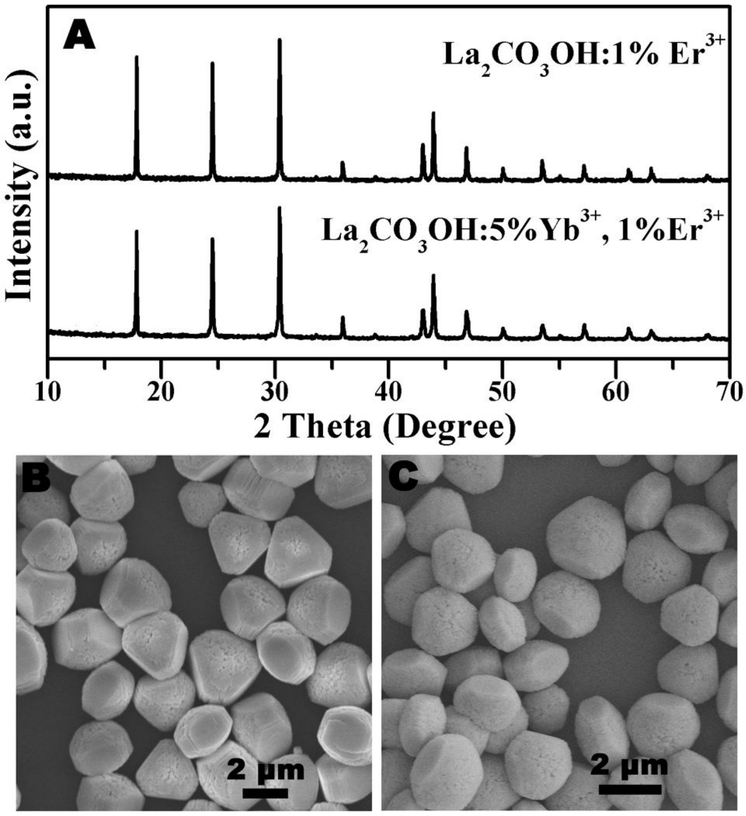

Figure S7. (A) XRD patterns of the as-prepared $LaCO_3OH$:1% Er^{3+} and $LaCO_3OH$:5% Yb^{3+}, 1% Er^{3+} products (pH = 10, V_{EG/H_2O} = 1:3, $C_{CO(NH_2)_2}$ = 6.25 mol·L^{-1}, the same experimental conditions to P18). (B) and (C) are the SEM images of $LaCO_3OH$:1% Er^{3+} and $LaCO_3OH$:5% Yb^{3+}, 1% Er^{3+}, respectively.

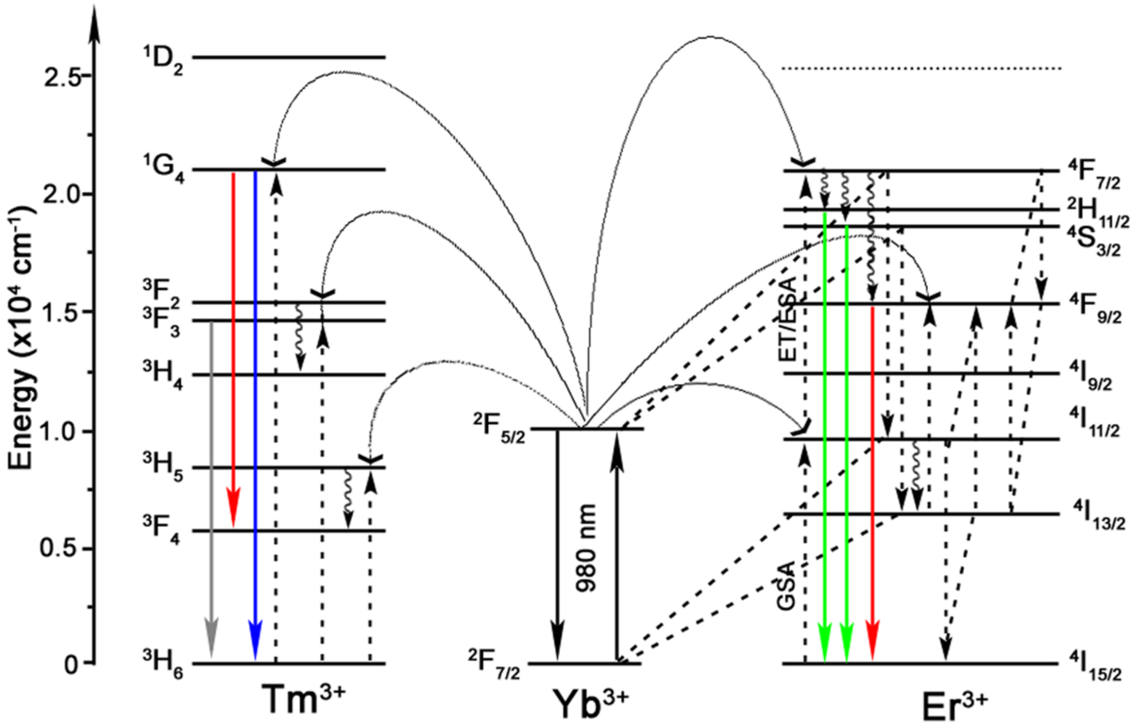

Figure S8. Energy level diagrams of the Yb^{3+}, Er^{3+}, and Tm^{3+} ions and the proposed UC emission mechanism.

Seen from **Figure S7**, the energy transfer occurs from the Yb^{3+} ion to Er^{3+} or Tm^{3+} ions. The blue-light emission of Tm^{3+} of $^1G_4$ energy level is accomplished by the three-step sequential ET from the excited Yb^{3+} to Tm^{3+}. First, absorption of pump photons populates the long-lived $^2F_{5/2}$ level in Yb^{3+}. Non-resonant ET from Yb^{3+} to Tm^{3+} causes excitation to the $^3H_5$ level in Tm^{3+}. This population relaxes rapidly to the $^3F_4$ level by nonradiative multiphonon decay. A second nonresonant ET from Yb^{3+} to Tm^{3+} populates the $^3F_2$ and $^3F_3$ levels, and subsequently multiphonon decay occurs leading to population of $^3H_4$ level. A third ET finally populates the $^1G_4$ level, then generates the emissions at 476 nm ($^1G_4 \rightarrow {}^3H_6$) (most strong), 653 nm ($^1G_4 \rightarrow {}^3F_4$) and 693 nm ($^3F_3 \rightarrow {}^3H_6$). In the Yb^{3+} and Er^{3+} codoped system, the green and red light emissions are predominantly due to the two-step ET from the excited Yb^{3+} to Er^{3+} and a little contribution from Er^{3+} ground/excited-state absorption (GSA/ESA). First, Yb^{3+} ions are excited from $^2F_{7/2}$ to $^2F_{5/2}$ level by 980 nm laser, and then the energy is transferred to Er^{3+} to populate $^4I_{11/2}$ level. During the population of the $^4I_{11/2}$ level, a second 980 nm photon transferred by the excited Yb^{3+} ions can populate a higher $^4F_{7/2}$ energetic state from $^4I_{11/2}$ of the Er^{3+} ions via energy transfer and excited-state absorption. The Er^{3+} ion can then relax nonradiatively by a fast multiphoton decay process to the $^2H_{11/2}$ and $^4S_{3/2}$ levels, and the dominant green $(^2H_{11/2} + {}^4S_{3/2}) \rightarrow {}^4I_{15/2}$ emissions (545, 557 nm) occur. On the other hand, the electron can further relax to the $^4F_{9/2}$ level, which relaxes radiatively to the ground-state $^4I_{15/2}$ level to generate red emissions (662, 671 nm). The Er^{3+} ion can also absorb 980 nm photons to populate $^4I_{11/2}$ level and then nonradiatively relax to $^4I_{13/2}$ level. The populated $^4I_{13/2}$ level might be excited to the $^4F_{9/2}$ red-emitting level in Er^{3+} ions by cross-relaxation process $^4I_{13/2} + {}^4I_{11/2} \rightarrow {}^4F_{9/2} + {}^4I_{15/2}$. In addition, the higher efficiency of the cross relaxation in Er^{3+} ions, that is, $^4F_{7/2} + {}^4I_{11/2} \rightarrow {}^4F_{9/2} + {}^4F_{9/2}$, which also can directly populate the $^4F_{9/2}$ red-emitting level. The energy transfer from Er^{3+} to Er^{3+} occurs with the enhancement of Er^{3+} content, so the electron is transferred again from $^4I_{13/2}$ to $^4F_{9/2}$ levels after adsorbing a photon from adjacent Er^{3+} ion. Subsequently, the electron radiatively relaxes to the ground state ($^4I_{15/2}$) from $^4F_{9/2}$ level and give the red emission. This process depopulates the $^2H_{11/2}/{}^4S_{3/2}$ levels and thus decreases the green emission.

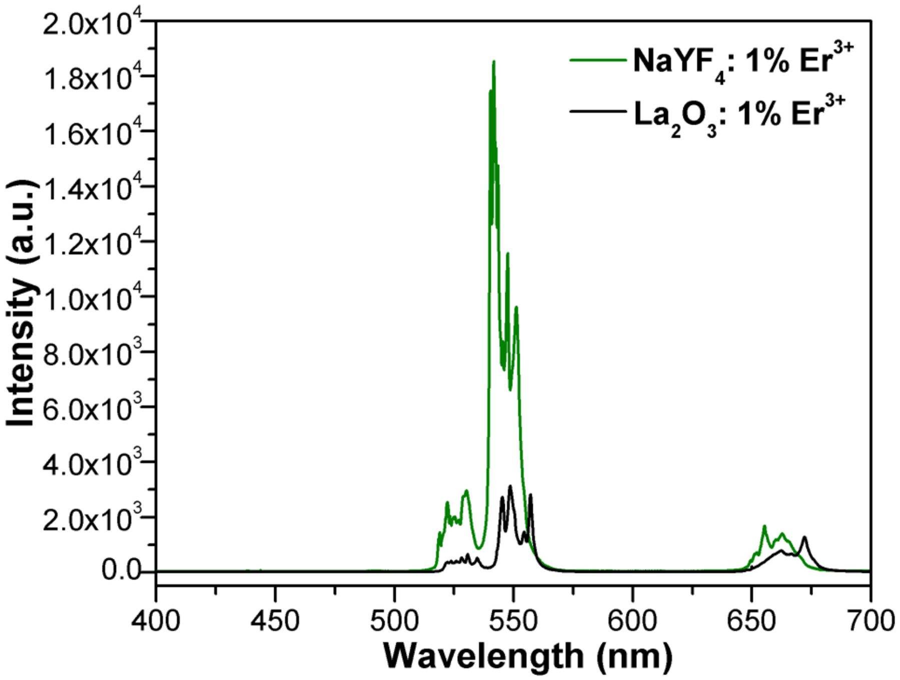

Figure S9. The UC emission spectra of La_2O_3:1% Er^{3+} and $NaYF_4$:1% Er^{3+} under the 980 nm LD excitation.